17th World Conference on Earthquake Engineering, 17WCEE
Sendai, Japan - September 13th to 18th 2020

A FUNDAMENTAL STUDY ON STRUCTURAL PERFORMANCE OF CES SHEAR WALLS WITH OPENINGS

S. SUZUKI[1]

[1] *Assistant Professor, Kochi University of Technology, suzuki.suguru@kochi-tech.ac.jp*

Abstract

The steel reinforced concrete (SRC) structures show good structural performance in terms of resisting lateral forces imposed by earthquakes in Japan. It has been adopted for medium-rise, high-rise, and super high-rise buildings. However, since the 1990s, the number of SRC buildings constructed has decreased. Although this decrease might be because of the development of a new structural engineering system called the high-strength concrete structure or concrete-filled steel tube structure, the main reason seems to be construction problems, which increase construction costs and lengthen construction schedules. Even so, it could be important that SRC structures provide the similar or better seismic performance than other structural systems. Therefore, the authors aim to develop a new structural system with a seismic performance as good as SRC structures, along with good workability, and have conducted a continuing development study on composite concrete encased steel (CES) structures composed of steel and fiber reinforced concrete. In the experimental study on CES columns, CES beam-column joints, a two-bay two-story CES frame, and CES shear walls, the CES structural system showed stable restoring force characteristics and good seismic performance.

On the other hand, openings such as windows and doors are placed in shear walls. The shear strength of RC shear walls with openings is generally evaluated using the strength reduction factor based on the opening area indicated in AIJ standard for RC structure in Japan. It is important to understand the structural performance of shear walls with openings and to verify the accuracy of shear strength evaluation in the CES structure.

In this study, static loading tests and three-dimensional FEM analyses were conducted to examine the structural performance and shear strength evaluation of CES shear walls with different opening areas.

The conclusions of this study is shown below.

1) The maximum capacity and initial stiffness of a large opening specimen were lower than that of a small opening specimen.

2) The shear strength evaluation method for RC shear walls with openings used in Japan underestimated the maximum capacity of CES shear walls with openings

3) As a result of FEM analyses, the diagonal compression struts were formed on the wall panel from the side of the opening to the bottom on the compression side and the top on the tensile side.

4) It is necessary to consider the effect of the boundary columns on the compression and tension sides in the shear resistance mechanism.

5) Modified Strut equation proposed on the above assumptions showed a good agreement with maximum capacity of CES shear walls with openings.

Keywords: CES shear walls, Static loading tests, FEM, Opening area, shear strength

1. Introduction

The steel reinforced concrete (SRC) structures show high performance in terms of resisting lateral forces induced by earthquakes in Japan. The SRC structures have been adopted for medium-rise, high-rise, and super high-rise buildings. However, the number of the constructed SRC buildings has decreased since the 1990s. Although the decrease may be due to the development of a new structural engineering system known as the high-strength concrete structure or concrete-filled steel tube structure, the main reason seems to be related to construction problems, such as high construction costs and long construction schedules. However, the SRC structures are still important as they can provide similar or better seismic performance than other structural systems.

Therefore, we aim to develop a new structural system with high workability and a seismic performance as good as the SRC structures. In this study, we conducted a continuing development study on the composite of the concrete encased steel (CES) structures composed of steel and fiber reinforced concrete (FRC). In previous experimental studies on CES columns, beam-column joints, two-bay two-story frames, and shear walls, the CES structural system was reported to show stable restoring force characteristics and high seismic performance [1-3].

Conversely, openings, such as windows and doors, are normally placed in shear walls. The shear strength of the reinforced concrete (RC) shear walls with openings is generally evaluated using the strength reduction factor, based on the opening area indicated in the Architectural Institute of Japan (AIJ) standard for RC structure in Japan [4]. Therefore, it is important to understand the structural performance of shear walls with openings and to verify the accuracy of shear strength evaluation in the CES structure.

In this study, static loading tests and three-dimensional Finite Element Method (FEM) analyses were conducted to examine the structural performance and shear strength of CES shear walls with different opening areas.

2. Test Procedure

2.1 Description of Specimens

In this study, the specimens were designed at one-third the scale of the prototype walls to simulate the lower stories of the multi-story shear walls in a high-rise building. In total, three specimens were prepared in this study.

Figs. 1 and 2 show, respectively, the configurations and bar arrangements of the specimens and Table 1 shows the details of the sections. For the prepared specimens, the floor height was 900 mm, the column span length was 1,800 mm, and the wall thickness was 100 mm. The boundary column had a square cross-

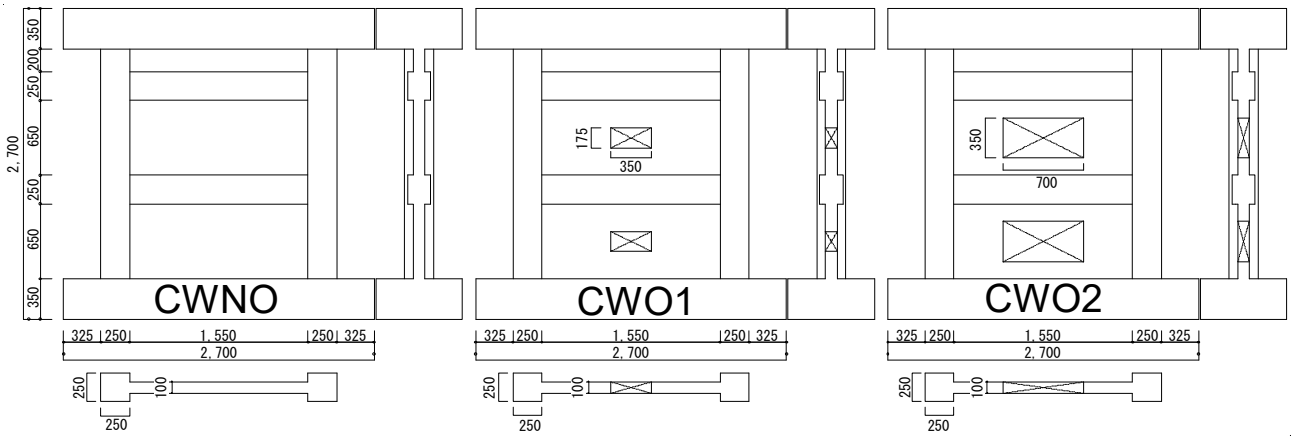

Fig. 1 – Configurations of specimens

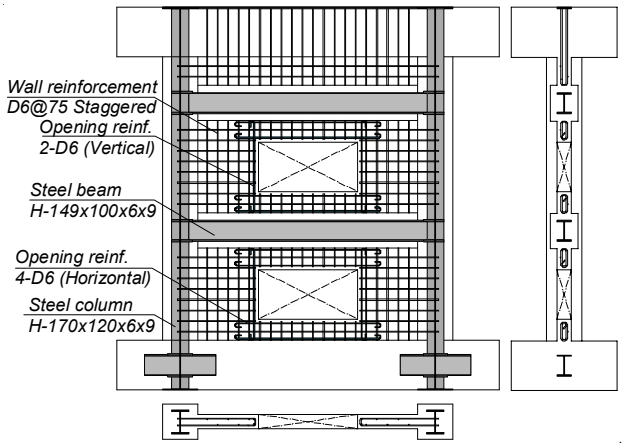

Fig. 2 – Arrangements of reinforcing bars (CWO2)

Table 1 – Details of specimens

		CWNO	CWO1	CWO2
Column	bxD	250×250		
	Steel	H-170×120×6×9 (p_s=4.9%)		
Beam	bxD	250×250		
	Steel	H-148×100×6×9 (p_g=5.2%)		
Wall panel	t_wxl_w	100×1,800		
	Reinforcement	D6@75 Zigzag (p_w=0.42%)		
Opening	h_{0p}xl_{0p}	-	175×350	350×700
	r_2	-	0.8	0.6
Others	Shear span ratio	0.9 (1,845mm)		
	Axial force	1,300kN (N/N_0=0.2)		

section with a length of 250 mm, and the boundary beam section was 200 × 250 mm. The longitudinal wall reinforcement for all specimens was bent in the wall panel as shown in Fig. 2. The transverse wall reinforcement for all specimens was welded to the steel web in the boundary column.

The open area is used as the variable in this study. Specimen CWNO was the non-opening shear wall. Specimens CWO1 and CWO2 were the shear walls with openings. The opening areas were varied according to the strength reduction factor r_2 described in the AIJ standard for RC structures [4]. The opening area was 175 × 350 mm for Specimen CWO1 and 350 × 750 mm for Specimen CWO2.

$$r_2 = 1 - 1.1 \times \sqrt{\frac{h_{0p} \cdot l_{0p}}{h \cdot l}} \tag{1}$$

where h, l, h_{0p}, and l_{0p} are the floor height, span length, opening height, and opening length, respectively.

2.2 Material Properties

The mechanical properties of the FRC and steel are shown in Tables 2 and 3, respectively. Poly vinyl alcohol (PVA) fibers with a diameter of 0.66 mm and length of 30 mm were used for the FRC. The volumetric ratio of the fibers was 1.0%.

2.2 Loading Program

Fig. 3 shows the loading apparatus used in this study. The wall specimens were loaded with horizontal cyclic shear forces using a hydraulic jack with a capacity of 2,000 kN while applying a constant axial force of 1,300 kN (N/N_0=0.2, where N is the axial load and N_0 is the axial load capacity of the steel of boundary columns) using two vertical manual jacks, with each having a capacity of 2,000 kN. During the test, an additional

Table 2 – Material properties of fiber reinforced concrete

	CWNO			CWO1			CWO2		
	1F	2F	3F	1F	2F	3F	1F	2F	3F
Compressive stress (N/mm^2)	37.5	34.7	50.2	35.3	41.5	47.2	49.5	47.1	48.5
Elastic modulus (kN/mm^2)	32.7	30.1	33.5	31.1	32.5	34.9	36.4	36.3	35.8

Table 3 – Material properties of steels

	H-170×120×6×9 (SS400)		H-170×120×6×9 (SS400)		D6 (SD295A)
	Web	Flange	Web	Flange	
Yield stress (N/mm^2)	309	330	311	292	324
Elastic modulus (kN/mm^2)	205	207.4	209.7	203.8	186.7

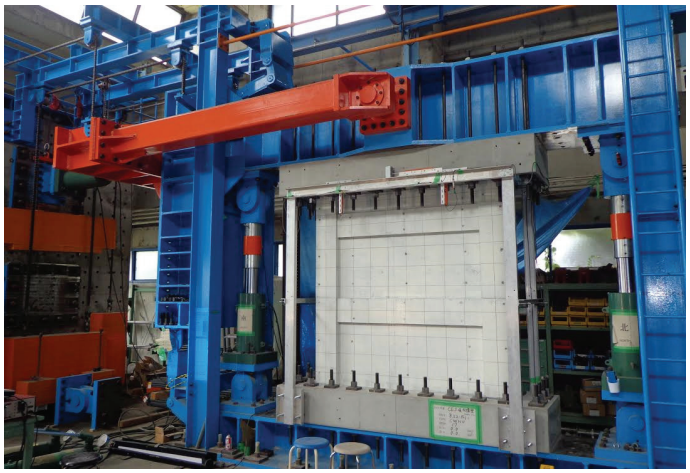

Fig. 3 – Loading apparatus

moment was applied to the top of the specimen by the two vertical manual jacks to maintain the prescribed shear-span ratio of 0.9 using the following equations:

$$N_s = \frac{N_c}{2} - \frac{Q}{l}(h-a) \tag{2}$$

$$N_n = \frac{N_c}{2} + \frac{Q}{l}(h-a) \tag{3}$$

where N_s is the axial force of the south jack; N_n is the axial force of the north jack; N_c is the constant axial force (1,300 kN); Q is the shear force; l is the distance between vertical jacks (4,000 mm); h is the assumed height of the applied shear force (1,845 mm); and a is the actual height of the applied shear force (2,700 mm).

Loading was conducted by controlling the relative drift angle (R) given by $R=\delta/h_0$, where δ is the horizontal deformation and h_0 (2,050 mm) is the height corresponding to the measuring point for the horizontal displacement at the top of the specimen. The horizontal loading sequences consisted of one cycle for R of 0.0625 and 0.125 $\times 10^{-2}$ rad, two cycles for R of 0.25, 0.5, 0.75, 1.0, 1.5, and 2.0 $\times 10^{-2}$ rad, and one cycle for R of 3.0 $\times 10^{-2}$ rad.

3. Test Results

Fig. 4 shows the cracking patterns of all specimens after the test. Fig. 5 shows the relationship between the shear force and drift angle, where the straight lines represent the calculated shear strength.

In Specimen CWNO with no openings, the horizontal slip, between the beam on the second floor and wall panel, occurred in the cycle of 1/200 rad. The maximum capacity reached 1,444 kN in the cycle of 1/200 rad. Then, a compressive failure of concrete occurred at the upper corner of the wall panel on the first floor; In Specimen CWO1 with small openings, the maximum capacity reached 1,376 kN in the cycle of

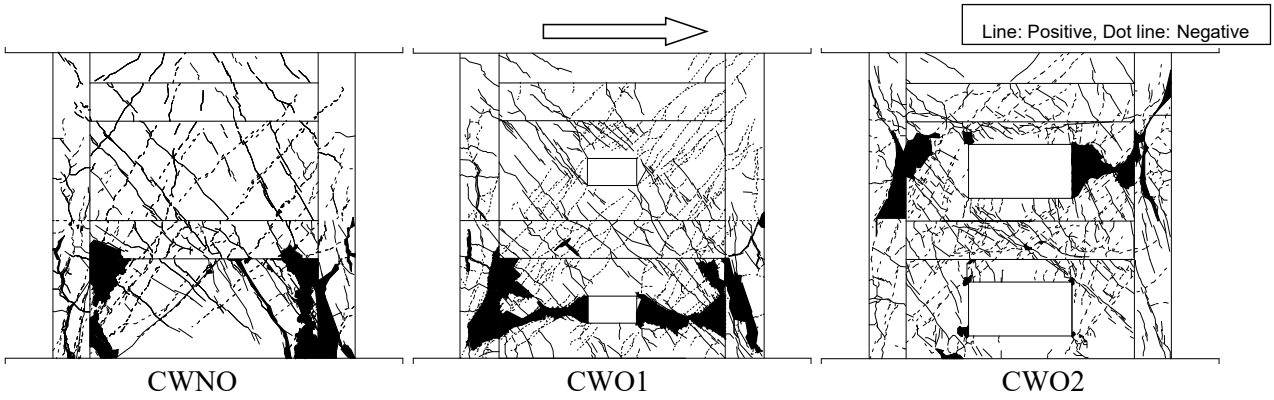

Fig. 4 – Failure modes at R of 1/33 rad.

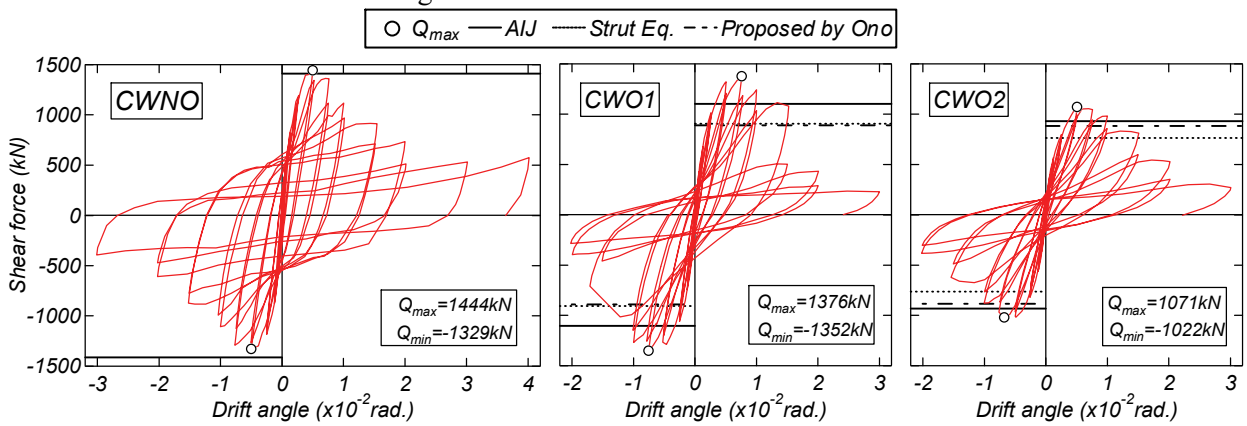

Fig. 5 – Shear force versus drift angle relationships

1/133 rad due to the compressive failure of the wall panel on both sides of the opening on the first floor. The strength deteriorated in the cycle of 1/67 rad due to the shear failure of the wall panel; In Specimen CWO2 with large openings, the maximum capacity reached 1,071 kN in the cycle of 1/200 rad, due to the compressive failure of the wall panel on both sides of the opening on the second floor. Then, the strength decreased gradually as the compressive failure progressed.

The ratio of the maximum capacity between Specimens CWO1 and CWNO was 0.95, and 0.74 between Specimens CWO2 and CWNO. These ratios were higher than the calculated strength reduction factor due to the opening, as shown in Eq. (1). Moreover, a decrease of the initial stiffness and an increase of the deformation capacity were observed as the opening area increased. This indicated that the specimen behavior was shifted from the shear wall to the frame, as the opening area increased.

4. Evaluation of Ultimate Strength

The compressive strength of the concrete on the first floor was used to calculate the strength of Specimens CWNO and CWO1. In contrast, the compressive strength of the concrete on the second floor was used to calculate the strength for Specimen CWO2, because the compressive failure occurred on the second floor.

Eq. (4) shows the bending strength equation for the CES shear walls. Eq. (5) shows the shear strength equation for the CES shear walls with no openings, based on the Truss-Arch theory. The shear strength of the CES shear wall with openings was calculated using three methods. The first method was by multiplying the Truss-Arch equation by the strength reduction factor due to the opening (Eq. (1)). The second method was using the Strut equation (Eqs. (6) and (7)) described in Ref. 5. The third method was by multiplying the strength reduction factor by the Slip equation proposed by Ono (Eqs. (8) and (9)).

Table 4 – Calculated results

		CWNO	CWO1	CWO2
Observed maximum capacity		1,444	1,376	1,071
Ultimate bending strength			1,604	
Truss Arch Equation x r_2	Calculated	1,421	1,108	929
	Obs. / Cal.	1.02	1.24	1.15
Strut Equation	Calculated	-	906	883
	Obs. / Cal.		1.52	1.21
Proposed Method by Ono	Calculated	1,082	890	765
	Obs. / Cal.	1.33	1.55	1.40

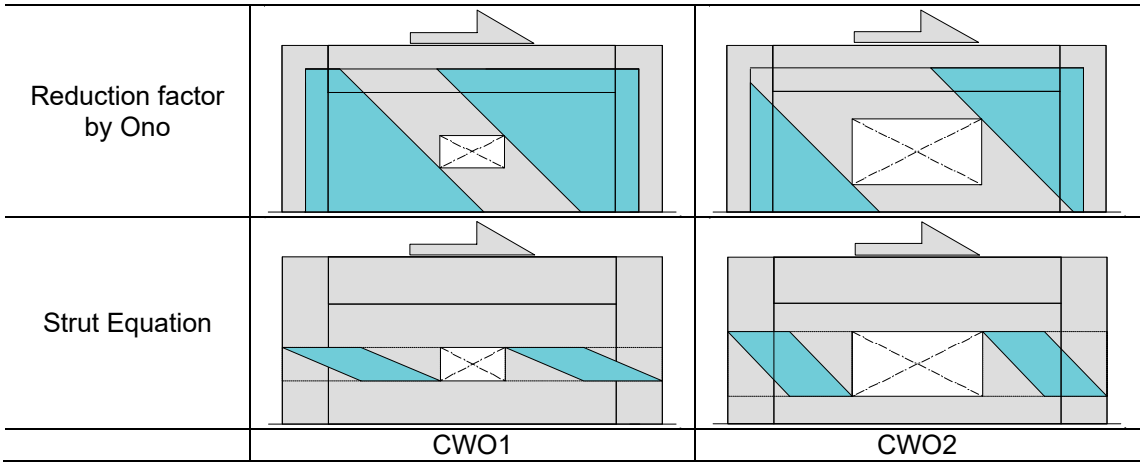

Fig. 6 – Shapes of compressive struts

<Ultimate bending moment[1)]>

$$Q_{mu} = \left(0.5N + {}_{sCS}A \cdot {}_{s}\sigma_{y}\right) l_w / h_w \tag{4}$$

<Truss·Arch equation[1)]>

$$Q_{su} = {}_{w}t\left\{ {}_{w}l_t \cdot p_{se} \cdot {}_{w}\sigma_{y} \cdot \cot\varphi + \tan\theta\left(1-\beta\right) {}_{w}l_a \cdot \nu \cdot \frac{\sigma_B}{2} \right\} \tag{5}$$

< Strut equation[2)] >

$$Q_{wo} = \sum 0.5\nu \cdot \sigma_B \cdot \cos\theta \cdot \sin\theta \cdot l_p \cdot t_p \tag{6}$$

$$\nu = -0.016\sigma_B - 0.16\frac{M}{Q \cdot L} + 0.36\frac{N}{b \cdot D \cdot \sigma_B} + 0.27 p_w + 1.23 \tag{7}$$

< Strength reduction factor proposed by Ono[6)] >

$$r_u = \sqrt{\frac{\sum A_e}{h \cdot l}} \tag{8}$$

< Slip strength equation[6)] >

$$Q_{u0} = \left(2.4\sqrt{F_c} + 3400 P_s\right) \cdot t l_w \ \text{(kgf)} \tag{9}$$

Table 4 shows the calculated and test results, and Fig. 6 shows the compressive strut shape assumed in the strut equation. The observed maximum capacity of Specimen CWNO with no openings can be evaluated by the Truss-Arch equation. Conversely, the calculated results, from the three methods in both specimens with openings, were lower than the observed maximum capacities. The calculated results obtained by the first method showed a relatively close agreement with the maximum capacities of specimens with openings.

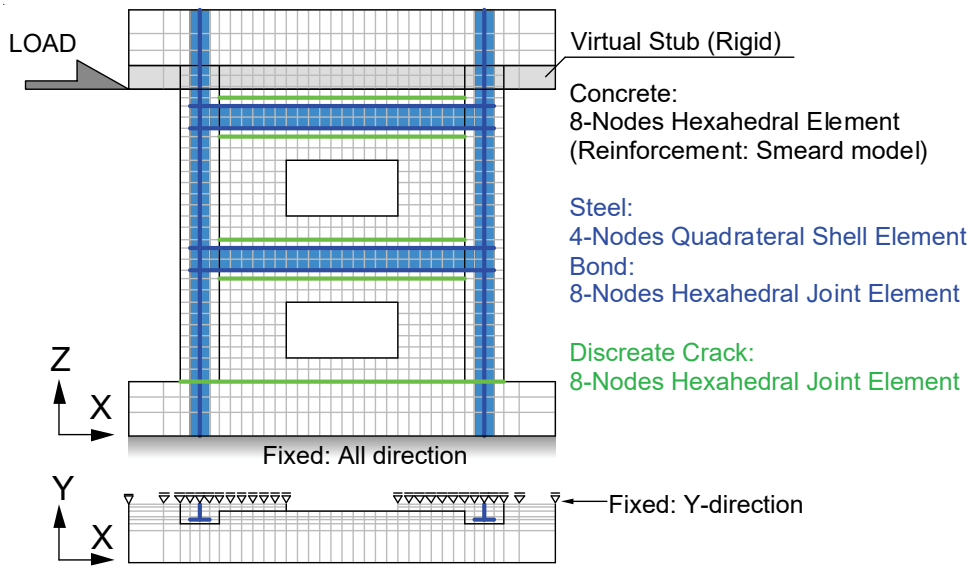

Fig. 7 – Finite Element Mesh layout

However, this method cannot consider the effects of the opening position and shape. The calculated results from the first and second method by Ono were significantly underestimated in specimens with openings.

5. Shear Transferring Mechanism

5.1 FEM Analyses

In this section, three-dimensional analyses were conducted for the CES shear walls with openings using the commercial software "FINAL". Fig. 7 shows the finite element mesh layout of Specimen CWO2. Because the specimen was symmetric in the out-of-plane direction, only one side in the out-of-plane direction of the specimens was modeled. Each node at the bottom end of the under stub was fixed to restrain the vertical and lateral displacement. The elements between the loading points had a prescribed shear span ratio of 0.9 and the bottom end of the upper stub were defined as an elastic body, which is a virtual stub. The node at the bottom of the virtual stub was subjected to lateral displacement reversals by applying a constant initial axial force of 1,300 kN.

Concretes were modeled by the 8-node hexahedral elements. Reinforcing bars in the wall panel were used to substitute the equivalent layers with stiffness in the bar direction and superposed on the hexahedral elements. For the stress-strain relationship of the FRC, the modified Ahmad model [7] was adopted in the stress-rising regions, and the stress-softening regions were simulated by a multi-linear model using the substantial data from the material tests, as shown in Fig. 8 (a). The 5-parameter model proposed by Ohnuma [8] was adopted as the fracture criterion of concrete under the tri-axial stress state. The tension stress was taken to be small after the crack occurred, and the concrete tension model proposed by Izumo [9] was used in the descending branch with the coefficient c of 0.4 for the wall panel and 1.0 for the CES frame (Fig. 8 (b)). The stiffness reduction due to the cyclic stress [10] was considered as shown in Fig. 7 (d). As a shear transfer model after cracks occurred in the FRC, the modified Al-Mahaidi model was adopted [11], where β was changed from 1.0 to 0.8 to decrease the shear transfer stiffness, as shown in Fig. 7 (d).

Steels were modeled by the 4-node quadrilateral elements. The material model of steel was a plasticity model that used the Von-Mises model failure surface with the associated plastic rule. The stress-strain curve of the steel was idealized by bi-linear model.

The 8-node hexahedral joint elements were used as the bond model between concrete and steel nodes.

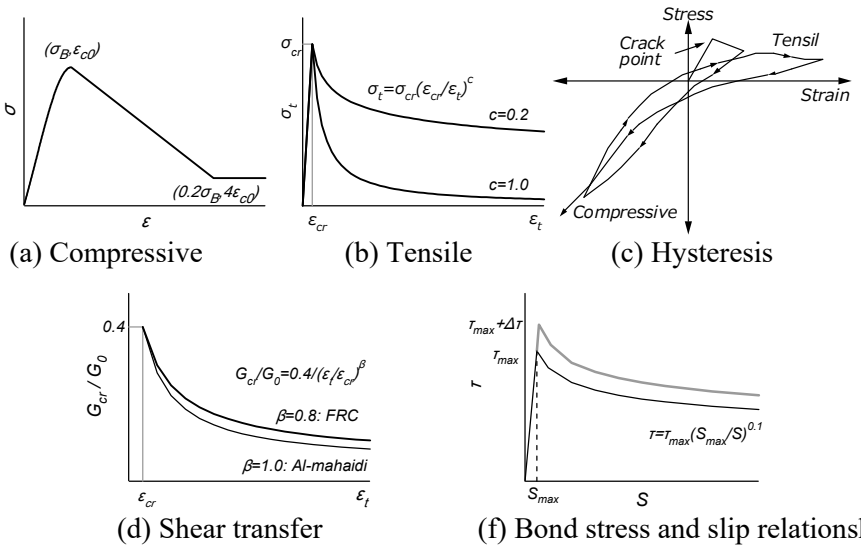

(a) Compressive (b) Tensile (c) Hysteresis

(d) Shear transfer (f) Bond stress and slip relationships

Fig. 8 – Constitutive laws

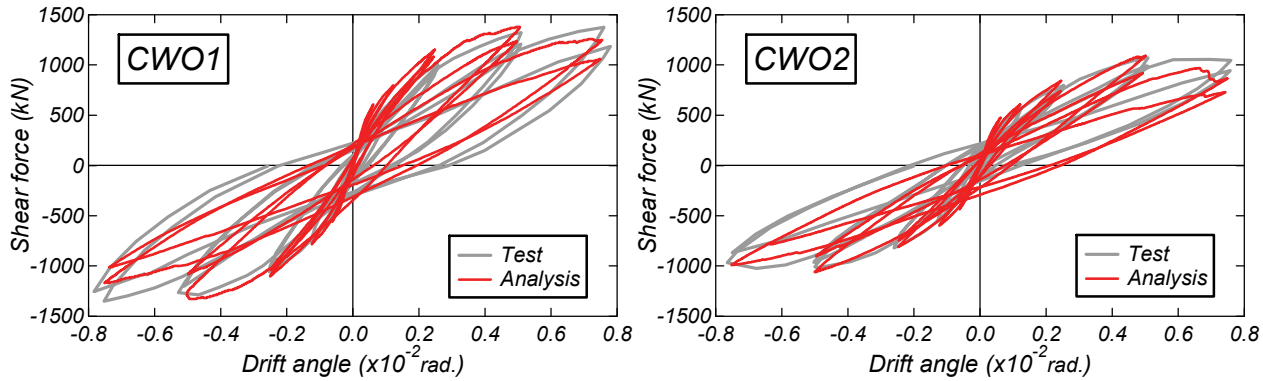

Fig. 9 – Shear force versus drift angle relationships

The relationship between the bond stress and slip was modeled using a multi-linear model [12], as shown in Fig. 8 (f). The maximum bond stress was 0.05 N/mm^2 and the slip at the maximum bond stress was 0.05 mm. In addition, the friction coefficient between the concrete and steel was 0.65. In contrast, discrete crack elements were adopted between the wall panel and beam or stub [13], and the tension stress was zero after cracking.

5.2 Analyses Results

Fig. 9 shows the comparison of the test and analysis results of the relationship between the shear force and drift angle. In both specimens, the strength deterioration of the analytical results was earlier than that of the test results. However, the analytical results of both specimens were found consistent with the test results until when *R* was 1/200 rad.

Fig. 10 shows the shear force for different shear and flexural displacement until *R* was 1/133 rad. The flexural displacement was calculated from the axial displacement of the boundary columns in both tests and analyses. The shear displacement subtracted the flexural displacement from the total horizontal displacement. In both analytical results, the shear displacement from the analysis was larger than the flexural displacement. The behavior of the flexural and shear displacement in the analysis corresponded with that in the test results.

From the above analysis, it was concluded that the analytical model for CES shear walls with the openings could generally reproduce the behavior of the test results.

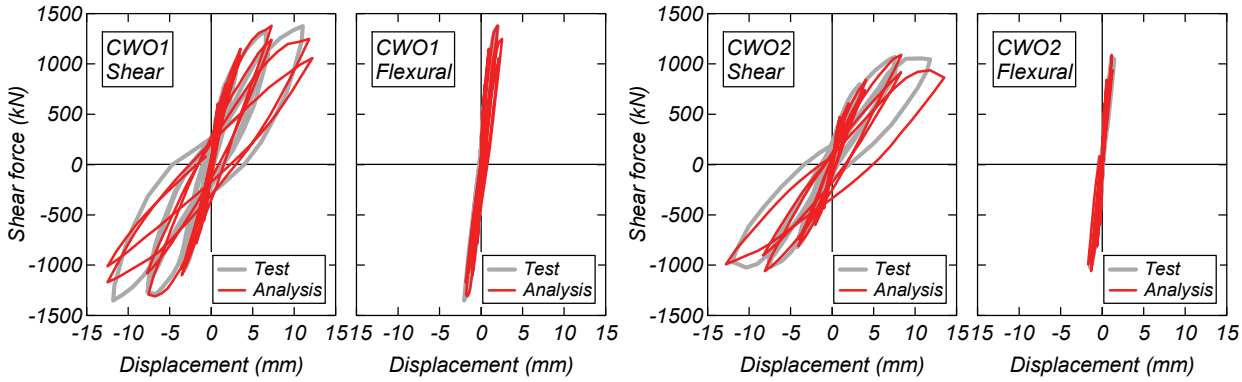

Fig. 10 – Deformation components

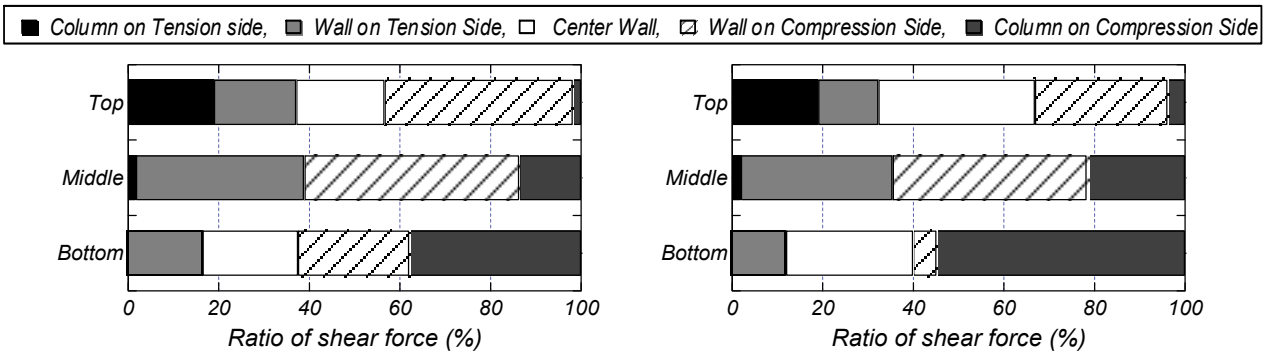

(a) Specimen CWO1 (b) Specimen CWO2

Fig. 11 – Height distributions of shear force contribution

5.3 Shear Force Contributions of Each Member

Fig. 11 shows the distribution of the shear force ratio for each member in the height direction. The shear force was divided into boundary columns, including the steel, wall panel on compression, tension side, and center side. The shear force was shown at the top, middle, and bottom of the wall panel. The shear force was calculated by multiplying the element area from the XZ-direction by the shear stress in the element. Fig. 11 shows the shear forces when the maximum capacities were reached in each specimen of the analysis.

In the middle part of the wall panel, the ratios of the shear forces on the compression side wall and column in both specimens were larger than those of the tension side wall and column. The total ratios of the shear force on the compression side of the wall panel and column in both specimens were almost the same in the middle and bottom parts. Further, the total ratios of the shear force on the tension side of the wall panel and column in both specimens were almost the same in the middle and top parts. This indicated that it is necessary to assume that the compressive struts for CES shear walls with openings were formed from the top of the wall panel to the bottom of the opening on the tension side wall panel; and the top of the opening to the bottom of wall panel on the compression side wall panel. In contrast, the shear force ratio on the tension side column at the top part was higher than that in the middle part, and the shear force ratio on the compression side column at the bottom part was higher than that at the middle part. Therefore, it is necessary to consider the effect of both boundary columns on the width of the compression struts.

5.3 Ultimate Shear Strength Evaluation

In this section, the Strut equation shown in Eq. (6) was Modified based on the shape of the compressive strut examined in the previous section. The calculated method of the shear strength for CES shear walls with the openings is called the modified Strut equation. Note that the effective strength factor v was not considered in the modified Strut equation.

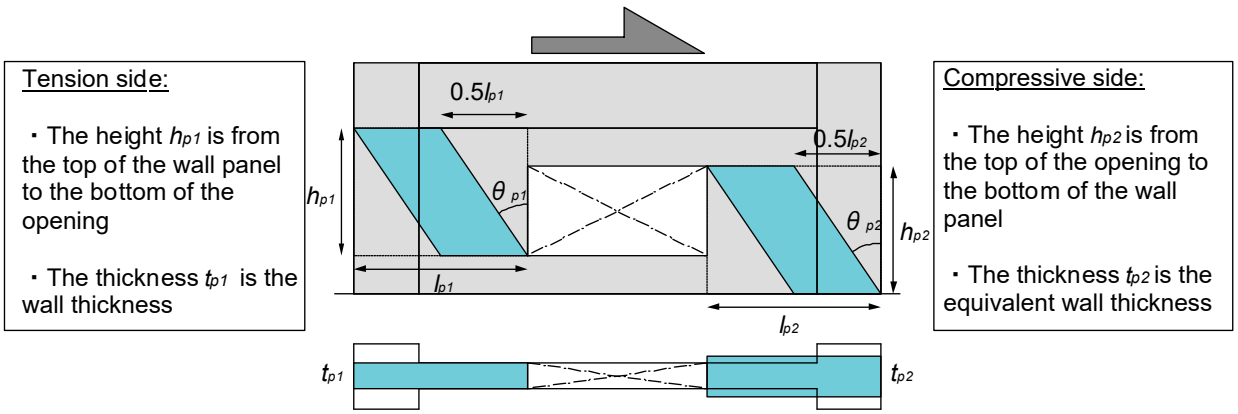

Fig. 12 – Proposed shape of compressive strut by modified Strut equation

Table 5 – Calculated results by modified Strut equation

	CWO1				CWO2			
	Tension	Compression	Total	Obs./Cal.	Tension	Compression	Total	Obs./Cal.
Observed strength	-		1,376	-	-		1,071	-
FEM	517	845	-	-	577	657	-	-
Strut equation	342	564	906	1.52	234	650	883	1.21
Modified-Strut equation	556	801	1,357	1.01	388	603	991	1.08

Fig. 12 shows the shape of the compressive strut for CES shear walls with the openings. The strut length l_{pi} and the strut height h_{pi} were assumed to be on the wall panel on both sides of the opening; the strut length l_{pi} was assumed to extend from the opening to the outer end of the columns; the strut height h_{pi} was assumed to extend from the top of the wall panel to the bottom of the opening on the tension side and from the top of the opening to the bottom of the wall panel on the compression side. In addition, the thickness of the compressive strut was replaced with the equivalent wall thickness on the compression side. This was the same for the wall panel on the tension side according to the Ref. [6].

Table 5 shows the calculated results using the modified Strut equation. The results of the FEM analyses in the table show the middle part of the wall panel as illustrated in Fig. 12. The calculated results using the modified Strut equation showed a good agreement with the observed results from the test. Specifically, the strut heights h_{pi} of both wall panels from the modified Strut equation were significantly different from those from the original Strut equation. The shear force contributions, on the compression and tension sides, were found higher in the modified Strut equation than in the original Strut equation.

5. Conclusions

In this study, static loading tests and three-dimensional FEM analyses were conducted for CES shear walls with openings to examine the shear strength. From the analytical and experimental analyses, the following conclusions can be drawn.

1. The maximum capacity and initial stiffness of wall specimens with large openings were lower than those of wall specimens with small openings were.
2. The shear strength evaluation method for RC shear walls with openings used in Japan was found to underestimate the maximum capacity of CES shear walls with openings
3. From the FEM analyses, the diagonal compression struts were formed on the wall panel from the side of the opening to the bottom of the compression side and top of the tensile side.
4. It is necessary to consider the effect of the boundary columns of the compression and tension sides in studying the shear resistance mechanism.

5. The modified Strut equation proposed, based on the above assumptions, showed a close agreement with the maximum capacity of the CES shear walls with openings.

6. References

[1] Suguru SUZUKI, Tomoya MATSUI and Hiroshi KURAMOTO (2012): A fundamental study on structural performance of CES shear walls with different anchorage condition of wall reinforcing bars, *Proceedings of 15th World Conference on Earthquake Engineering*, **961**

[2] Suguru SUZUKI and Hiroshi KURAMOTO (2014): Non-linear FEM analysis for CES shear walls, *Proceedings of 10th U.S. National Conference on Earthquake Engineering*, **113**

[3] Suguru SUZUKI, Hiroshi KURAMOTO and Tomoya MATSUI (2015): Restoring force characteristics model of CES shear walls, *Proceedings of 11th Canadian Conference on Earthquake Engineering*, **93798**

[4] Architectural Institute of Japan (2010): AIJ Standard for Structural Calculation of Reinforced Concrete Structure

[5] Masato SAKURAI, Hiroshi KURAMOTO and Tomoya MATSUI (2012): Shear strength evaluation for RC shear walls with multi-openings based on FEM analysis, *Proceedings of 15th World Conference on Earthquake Engineering*, **797**

[6] Masayuki ONO and Ikuo HOKUHIRO (1992): A proposal of reducing rate for strength due to opening effect of reinforced concrete framed shear walls, *Journal of Structural and Construction Engineering (Transactions of AIJ)*, **435**, 119-129

[7] Kazuhiro NAGANUMA (1995): Stress-strain relationships for concrete under triaxial compression. *Journal of structural and construction engineering (Transactions of AIJ)*, **474**, 163-170.

[8] Hiroshi. Ohnuma and Masao AOYAGI (1981): Ultimate strength properties of concrete under triaxial compressive stresses, *CRIERI Research Report*, **381021**, (in Japanese)

[9] Junichi IZUMO, Hyunmock Shin, Koichi MAEKAWA and Hajime OKAMURA (1989): Analytical model for a reinforced concrete panel element subjected to reversed cycle in-plane stresses. *Journal of structural mechanics and earthquake engineering*, **408**, 51-60.

[10] Kazuhiro NAGANUMA, Masaaki OHKUBO (2000): An analytical model for reinforced concrete panels under cycle stresses. Journal of structural and construction engineering *(Transactions of AIJ)*, **536**, 135-142 (in Japanese)

[11] Riadh Saleh Hassan Al-Mahaidi (1979): Nonlinear finite element analysis of reinforced concrete deep members, Dep. of Structural Engineering, Cornell Univ., **79-1**

[12] Osamu AMANO, Hikaru NAKAMURA, Takeshi HIGAI and Hirokazu TANAKA (1998): Shear behavior analysis of steel-tube concrete composite columns, *Proceedings of the Japan Concrete Institute*, **20** (3), 823-828 (in Japanese)

[13] Tetsuya MISHIMA, Kazuie YAMADA and Koichi MAEKAWA (1992): Localized deformational behavior of a crack in RC plates subjected to reversed cyclic loads, *Journal of Japan Society of Civil Engineers*, **442**, 161-170 (in Japanese)

